Journal of Network and Innovative Computing
ISSN 2160-2174 Volume 1 (2013) pp. 109 -118

Source Number Estimation in Shallow Ocean by Gerschgorin Disks Using Acoustic Vector Sensor Array

N Suresh Kumar[1], Dibu John Philip[2] and G V Anand[3]

[1]Naval Physical and Oceanographic Laboratory
Kochi 682021, India
sureshkumarnpol@yahoo.co.in

[2]Rajagiri School of Engineering and Technology
Kochi 682039, India
dibujphilip@ieee.org

[3]Indian Institute of Science
Bangalore 560012, India
anandgv@ece.iisc.ernet.in

Abstract: **Estimating the number of sources accurately plays a crucial role in the source localization and direction of arrival (DOA) estimation problems. Source number estimation has to be performed in a shallow ocean environment in several applications like coastal surveillance and harbour defence. Also, it is desirable to have an array of very short length so as the reduce the drag force experienced when used along with autonomous underwater vehicles (AUV). In this paper, the Gerschgorin disk estimator (GDE) method of source number estimation in an unbounded medium is extended for operation in a shallow oceanic waveguide. Classical methods of source number estimation such as Akaike information criterion (AIC) and minimum description length (MDL) require (1) good estimates of the eigenvalues of the spectral correlation matrix, and (2) the assumption of white Gaussian noise to be valid. The GDE method does not suffer from these limitations. A theoretical formulation of the GDE method in a shallow ocean is presented in this paper for acoustic vector sensor (AVS) and acoustic pressure sensor (APS) arrays. Simulation results are then presented considering different noise models including non-Gaussian and highy correlated noise to illustrate the advantages of the GDE method and the superior performance of the AVS array in a shallow ocean environment.**

Keywords: Gerschgorin disk estimator, acoustic vector sensor array, shallow ocean.

I. Introduction

Passive localization of acoustic sources in shallow ocean is a problem of great interest in applications such as coastal surveillance and harbour defence. High-resolution direction of arrival (DOA) estimation algorithms such as MUSIC [1] and ESPRIT [2], rely on prior knowledge of the number of sources. It is therefore necessary to have a reliable method of source number estimation. Classical methods of source number estimation include the Akaike information criterion (AIC) method [3], the minimum description length (MDL) method [4], and several variants derived from them. These are model-dependent estimators based on the assumption that noise is Gaussian, and temporally and spatially white. But, in the ocean environment, ambient noise is often impulsive [5], [6] and the noise at the sensors of a vertical array is correlated [7]. Moreover, these methods require knowledge of the eigenvalues of the array data covariance matrix. The accuracy of eigenvalue estimates, obtained from a finite number of snapshots, decreases as the signal-to-noise ratio (SNR) and / or the sample size (number of snapshots) is reduced. Hence the AIC and MDL estimators fail to correctly estimate the number of sources in the ocean in many cases of practical interest.

The Gerschgorin disk estimator (GDE) is a geometrical technique of source number estimation which was formulated by Wu et al [8], and developed further by Huang et al [9]. The GDE is (1) not restricted by the assumption of white Gaussian noise, and (2) robust to errors in estimation of eigenvalues of the covariance matrix. The GDE was originally developed for use with an array of scalar sensors such as acoustic pressure sensors (APS). This estimator was designated as GDE-P by

Mei and Wang [10], who formulated an extended version of the algorithm called GDE-V for use with an acoustic vector sensor (AVS) array. An AVS measures acoustic pressure as well as three orthogonal components of particle velocity at any given location, and thus it can provide directional information about a source. In general, an AVS array with a small number of sensors can achieve better source localization than an APS array with a larger number of sensors [11], [12], [13]. In the context of source number estimation, simulation results in [10] indicate that the performance of GDE-V is significantly better than that of GDE-P in terms of several performance measures, viz. probability of correct estimation at low SNR and/or small sample size, capacity for correct enumeration of a large number of sources, resolution of closely spaced sources, and elimination of left-right ambiguity.

The signal model considered in [8], [9], [10] is based on the assumption that the signal from each source arrives at the sensor array in the form of a plane wave. This assumption is not valid in the multi-mode environment of a shallow ocean. For example, the plane wave assumption leads to biased DOA estimates in a shallow ocean environment [14]. Therefore, the GDE-P and GDE-V methods cannot be used in their present form for source number estimation in a shallow ocean. In this paper, we have extended the GDE-P and GDE-V algorithms to a shallow ocean environment. In a shallow range-independent ocean, the acoustic pressure as well as each component of particle velocity can be expressed as the sum of a discrete set of normal modes [13], [15]. The AVS array data model for shallow ocean developed in [13] has been used in this paper. Uniform horizontal linear array (HLA) and vertical linear array (VLA) configurations have been considered. According to the noise model presented in [13], noise may be assumed to be spatially uncorrelated in the case of HLA if the inter-sensor distance is greater than or equal to half-wavelength. But noise is spatially correlated in the case of VLA. We have applied the GDE-P and GDE-V algorithms to the APS and AVS array data respectively, and shown that the performance of an AVS array is significantly better than that of an APS array. It is also shown that the performance of an HLA is much better than that of a VLA. We have also compared the performance of the GDE-V method with the AIC and MDL methods for an AVS array, and shown that (1) in white noise, the performance of GDE-V is better than that of the other algorithms at low SNR and/or small sample size, and (2) GDE-V is robust to temporal/spatial correlation of noise unlike the AIC and MDL algorithms. A part of this work was presented at the 12^{th} International Conference on System Design and Applications ISDA 2012 [16].

The outline of the paper is as follows. In Section II, we present a summary of the AVS and APS array measurement models for a horizontally stratified, range-independent shallow ocean. A review of the GDE algorithm is presented in Section III. Simulation results presented in Section IV are obtained by applying the GDE-P and GDE-V algorithms to the data models described in Section II. Section V concludes the paper.

II. Data Models For AVS and APS Array in Shallow Ocean

A. Signal Model

The ocean is modeled as a range-independent channel having a water column of depth h, density ρ, and sound speed c over a fluid half-space of density ρ_b and sound speed c_b. We consider HLA and VLA configurations of a uniform N-sensor AVS array with inter-sensor spacing d. Let the depth of the n^{th} sensor be denoted by z_n, $n = 1, \ldots, N$. We have $z_n = z_1$ for the HLA and $z_n = z_1 + (n-1)d$ for the VLA. Let J narrowband sources of center frequency f be located in the far-field region at range $r^{(j)}$, depth $z^{(j)}$, and bearing $\theta^{(j)}$. In the case of the HLA, the bearing is measured with respect to the axis of the array. Each AVS measures acoustic pressure p and three mutually orthogonal components of particle velocity (v_x, v_y, v_z) in the horizontal (x, y) and vertical (z) directions. We shall ignore the vertical component v_z since simulation results show that inclusion of v_z does not have a significant effect on the performance of any source enumeration algorithm. Hence the measurement at each AVS is considered to be 3-dimensional vector. Using the normal mode theory of sound propagation, the array signal vector due to the j^{th} source can be written as the following $3N$-dimensional vector

$$\begin{aligned}\mathbf{s}^{(j)} = [&p_1^{(\mathrm{j})}\ \sqrt{2}\rho c v_{x1}^{(j)}\ \sqrt{2}\rho c v_{y1}^{(j)}\ \ldots \\ &p_N^{(\mathrm{j})}\ \sqrt{2}\rho c v_{xN}^{(j)}\ \sqrt{2}\rho c v_{yN}^{(j)}]^{\mathrm{T}}\end{aligned} \tag{1}$$

for j=1, …, J, where $p_n^{(j)}, v_x n^{(j)}, v_y n^{(j)}$ denote, respectively, the complex amplitudes of the acoustic pressure and the (x, y) components of particle velocity at the n^{th} sensor when a unit-amplitude signal is transmitted by the j^{th} source. In (1), the particle velocity components are scaled by the factor $\sqrt{2}\rho c$ to maintain dimensional uniformity of the measured quantities and also to ensure that the three components of noise at an AVS have equal variance. Expressions for $p_n^{(j)}, v_x n^{(j)}$ and $v_y n^{(j)}$ are given by [13]

$$p_n^{(\mathrm{j})} = \sum_{m=1}^{M} p_{mn}^{(j)} \Omega(\theta^{(j)}), \tag{2}$$

$$\sqrt{2}\rho c v_{xn}^{(j)} = \sqrt{2}\cos\theta^{(j)} \sum_{m=1}^{M} \frac{k_m}{k} p_{mn}^{(j)} \Omega(\theta^{(j)}), \tag{3}$$

and

$$\sqrt{2}\rho c v_{yn}^{(j)} = \sqrt{2}\sin\theta^{(j)} \sum_{m=1}^{M} \frac{k_m}{k} p_{mn}^{(j)} \Omega(\theta^{(j)}), \tag{4}$$

where

$$p_{mn}^{(j)} = \frac{2\sqrt{2\pi}}{h} \Psi_m(z_n) \Psi_m(z^{(j)}) \frac{e^{ik_m r^{(j)}}}{\sqrt{k_m r^{(j)}}}. \tag{5}$$

In (2) - (5), $\Psi_m(z)$ and k_m denote, respectively, the eigen-function and wave-number of the m^{th} normal mode of the

channel at frequency f, M is the total number of modes at this frequency, $k = \frac{2\pi f}{c}$, and $\Omega(\theta^{(j)})$ is defined as

$$\Omega(\theta^{(j)}) = e^{i(n-1)k_m d\cos\theta^{(j)}} \text{ for HLA,} \tag{6a}$$

$$\Omega(\theta^{(j)}) = 1 \text{ for VLA.} \tag{6b}$$

Let $\eta^{(j)}(t)$ be the complex amplitude of the signal transmitted by the j^{th} source at time t. The amplitudes $\{\eta^{(j)}(t); j = 1,,J; t = 1,2,\}$ are modeled as uncorrelated complex circular Gaussian random variables with mean $\mathrm{E}[\eta^{(j)}(t)] = 0$ and variance $\mathrm{E}[|\eta^{(j)}(t)|^2] = \sigma^{2(j)}$. Define $\mathbf{S} = [\mathbf{s}^{(1)} \dots \mathbf{s}^{(J)}]$, and $\boldsymbol{\eta}(t) = [\eta_1(t) \dots \eta_J(t)]^T$. The array data vector inclusive of the received signals from all sources and additive noise can be written as

$$\mathbf{y}(t) = \mathbf{S}\boldsymbol{\eta}(t) + \mathbf{w}(t), \tag{7}$$

where $\mathbf{w}(t)$ is the noise vector.

In the case of an APS array, the vector $s^{(j)}$ defined in (1) reduces to

$$\mathbf{s}^{(j)} = \mathbf{p}^{(j)} \triangleq [p_1^{(j)} \dots p_N^{(j)}] \tag{8}$$

and the data vector $\mathbf{y}(t)$ and the noise vector $\mathbf{w}(t)$ reduce to N-dimensional vectors.

B. Noise Model

It is convenient to express the array noise vector as $\mathbf{w}(t) = [\mathbf{w}_1^T(t) \dots \mathbf{w}_N^T(t)]^T$, where $\mathbf{w}_n(t) = [w_{n1}(t) w_{n2}(t) w_{n3}(t)]^T$ denotes the 3-dimensional noise vector at the n^{th} AVS. The noise is modeled as complex circular with a generalized Gaussian (GG) distribution. The probability density function (PDF) of a complex circular GG random variable $W = \bar{W} + i\tilde{W}$ with variance σ^2 is given by

$$f_W(w) = f_{\bar{W},\tilde{W}}(\bar{w},\tilde{w}) = B(\alpha)\exp\left(-C(\alpha)|w|^{\alpha}\right)$$

$$= B(\alpha)\exp\left(-C(\alpha)(\bar{w}^2+\tilde{w}^2)^{\alpha/2}\right), \tag{9}$$

where

$$B(\alpha) = \frac{\alpha\Gamma(4/\alpha)}{8\pi\sigma^2\Gamma(2/\alpha)^2},$$

$$C(\alpha) = \frac{1}{\sigma^{\alpha}}\left(\frac{\Gamma(4/\alpha)}{\Gamma(2/\alpha)}\right)^{\alpha/2}.$$

Details of derivation of the expression in (9) are given in A. The GG distribution, which is Gaussian for $\alpha = 2$ and leptokurtic (heavy-tailed) for $\alpha < 2$, can model a wide variety of ambient noise environments in the ocean.

For a given time t, the three components of noise at an AVS are uncorrelated and identically distributed [13]. But the noise at different sensors is correlated with a depth-dependent variance. Let the covariance matrix of the noise vector $\mathbf{w}(t)$ be denoted by

$$\mathbf{R_w} = E[\mathbf{w}(t)\mathbf{w^H}(t)] = \sigma^2\mathbf{R_0}, \tag{10}$$

where σ^2 is the noise variance at the reference depth z_1, and $\mathbf{R}_0$ is a $3N \times 3N$ matrix. The spatial correlation decays rapidly in the horizontal direction, and it can be ignored for horizontal separations greater than or equal to half-wavelength. But the vertical spatial correlation between similar components of noise remains significant even at large distances. Hence, for an HLA at depth z_1, $\mathbf{R}_0$ is the $3N \times 3N$ identity matrix:

$$\mathbf{R}_{0,H} = \mathbf{I}_{3N}. \tag{11}$$

For a VLA, the matrix $\mathbf{R}_0$ is given by

$$\begin{bmatrix} r(z_1,z_z) & \dots & r(z_1,z_N) \\ \vdots & \ddots & \vdots \\ r(z_N,z_1) & \dots & r(z_N,z_N) \end{bmatrix} \otimes \mathbf{I}_3, \tag{12}$$

where $\otimes$ denotes the Kronecker product and

$$r(z_k,z_n) = \frac{\sum_{m=1}^{M}\Psi_m(z_k)\Psi_m(z_n)}{\sum_{m=1}^{M}\Psi_m^2(z_1)}. \tag{13}$$

It follows from (10), (12) and (13) that the noise variance at the n^{th} sensor of a VLA is given by

$$\sigma_n^2 = \sigma^2\frac{\sum_{m=1}^{M}\Psi_m(z_n)}{\sum_{m=1}^{M}\Psi_m^2(z_1)} \tag{14}$$

for $n = 1,\dots,N$.

We consider two models of temporal noise correlation. In the first model, noise is assumed to be temporally white. In the second model, noise is assumed to be colored and is modeled as an AR(1) process.

The SNR for the *j*-th source is defined as

$$(SNR)^{(j)} = \frac{\sigma^{(j)2}\mathbf{p}^{(j)H}\mathbf{p}^{(j)}}{N\sigma^2}, \text{ for HLA,} \tag{15a}$$

$$(SNR)^{(j)} = \frac{\sigma^{(j)2}\mathbf{p}^{(j)H}\mathbf{p}^{(j)}}{\sum_{n=1}^{N}\sigma^2}, \text{ for VLA.} \tag{15b}$$

This definition of SNR, based only on the acoustic pressure components of signal and noise, ensures a fair comparison of the performance of APS and AVS arrays.

The AVS array data covariance matrix is given by

$$\mathbf{R}_{3N} = E[\mathbf{y}(t)\mathbf{y}(t)^H]. \tag{16}$$

The true covariance matrix defined in (16) is estimated from Q snapshots of the data vector as follows:

$$\hat{\mathbf{R}}_{3N} = \frac{1}{Q}\sum_{t=1}^{Q}\mathbf{y}(t)\mathbf{y}(t)^H. \tag{17}$$

In the case of an APS array, the vector $\mathbf{y}$(t) is N-dimensional, the covariance matrix is $\mathbf{R}_N$ and its estimate is denoted by $\hat{\mathbf{R}}_N$.

III. Gerschgorin Disk Estimator

According to the Gerschgorin disk theorem, the eigenvalues λ of a square matrix $\mathbf{R}$ of dimension *N*-by-*N* belong to the union of *N* Gerschgorin disks; i.e.,

$$\lambda \in \bigcup_{i=1}^{N} O_i, \tag{18}$$

where each Gerschgorin disk O_i is defined in the complex plane as

$$O_i : |Z - c_{ii}| < c_i, \tag{19}$$

and

$$c_i = \sum_{j=1, j\neq i}^{N} |c_{ij}|, \tag{20}$$

in which c_{ij} is the element at the *i*-th row and *j*-th column of $\mathbf{R}$. Thus, i^{th} Gerschgorin disk is a circle centred at c_{ii} with radius c_i. But, the Gerschgorin theorem cannot be applied directly to the sample covariance matrix $\hat{\mathbf{R}}_{3N}$ to estimate the number of sources, because the disks are tightly interlaced and the radii c_i are so large that the signal and noise subspaces cannot be distinguished [8]. To circumvent this problem, a unitary transformation of the sample covariance matrix has been proposed [8]. Gerschgorin theorem can be applied to the transformed matrix since the eigenvalues of the original matrix are preserved by the unitary transformation.

Let the covariance matrix $\hat{\mathbf{R}}_{3N}$ be partitioned as

$$\hat{\mathbf{R}}_{3N} = \begin{bmatrix} \hat{\mathbf{R}}_{3(N-1)} & \mathbf{r} \\ \mathbf{r}^H & \mathbf{b}_3 \end{bmatrix}, \tag{21}$$

where $\hat{\mathbf{R}}_{3(N-1)}$ is the covariance matrix of order 3(N-1) corresponding to the array formed by the first $N-1$ sensors. An eigen-decomposition of the matrix $\hat{\mathbf{R}}_{3(N-1)}$ is carried out to obtain the matrix $\mathbf{U}_{3(N-1)}$=$[\mathbf{e}_1, \mathbf{e}_2, \ldots, \mathbf{e}_{3(N-1)}]$ that is formed by the set of unit eigenvectors orthogonal to each other. Next, the following unitary transformation matrix $\mathbf{T}$ is constructed:

$$\mathbf{T} = \begin{bmatrix} \mathbf{U}_{3(N-1)} & \mathbf{O}_3 \\ \mathbf{O}_3^T & \mathbf{I}_3 \end{bmatrix}, \tag{22}$$

where $\mathbf{O}_3$ is an all-zero matrix and $\mathbf{I}_3$ is the 3×3 identity matrix. Now, the transformed matrix $\mathbf{R}_T$ is defined as

$$\mathbf{R}_T = \mathbf{T}^H \hat{\mathbf{R}}_{3N} \mathbf{T} = \begin{bmatrix} \mathbf{\Sigma} & \mathbf{\Gamma} \\ \mathbf{\Gamma}^H & \mathbf{B}_3 \end{bmatrix}; \tag{23}$$

or $\mathbf{R}_T =$

$$\begin{bmatrix} \lambda_1 & 0 & \ldots 0 & \Gamma_{11} & \Gamma_{12} & \Gamma_{13} \\ 0 & \lambda_2 & \ldots 0 & \Gamma_{21} & \Gamma_{22} & \Gamma_{23} \\ \vdots & \vdots & \vdots \; \vdots & \vdots & \vdots & \vdots \\ 0 & 0 & \ldots \lambda_{3(N-1)} & \Gamma_{3(N-1),1} & \Gamma_{3(N-1),2} & \Gamma_{3(N-1),3} \\ \Gamma_{11}^* & \Gamma_{21}^* & \ldots \Gamma_{3(N-1),1}^* & \mathrm{B}_{11} & \mathrm{B}_{12} & \mathrm{B}_{13} \\ \Gamma_{12}^* & \Gamma_{22}^* & \ldots \Gamma_{3(N-1),2}^* & \mathrm{B}_{21} & \mathrm{B}_{22} & \mathrm{B}_{23} \\ \Gamma_{13}^* & \Gamma_{23}^* & \ldots \Gamma_{3(N-1),3}^* & \mathrm{B}_{31} & \mathrm{B}_{23} & \mathrm{B}_{33} \end{bmatrix}. \tag{24}$$

The diagonal matrix $\mathbf{\Sigma}$ contains eigenvalues of the matrix $\hat{\mathbf{R}}_{3(N-1)}$ such that $\lambda_1 \geq \lambda_2 \cdots \geq \lambda_J \geq \lambda_{J+1} = \cdots = \lambda_{3(N-1)}$. As $\mathbf{T}$ is a unitary matrix, the eigenvalues of $\mathbf{\Sigma}$ are the same as those of $\hat{\mathbf{R}}_{3(N-1)}$, and it has been shown in [8] that the Gerschgorin disks of the transformed matrix have radii Γ_i and centers λ_i where,

$$c_i = \sum_{j=1}^{3} |\Gamma_{ij}|, \tag{25}$$

i=1, 2, …, 3(N-1).

In theory, with an infinite number of samples, the radii of the disks associated with the noise subspace are zero, whereas those of the disk associated with the signal subspace are non-zero. In practice, as the number of samples is finite, a set of disks with large radii is chosen for the signal subspace, which is distinct from a second set of disks with small radii associated with the noise subspace. The union of the larger signal disks contains $\hat{J}$ eigenvalues, while the union of the smaller noise disks contains $3N$-$\hat{J}$ eigenvalues, where $\hat{J}$ is the estimated number of sources. To estimate the number of sources, we order the radii of the disks in descending order, so that $\Gamma_1 \geq \Gamma_2 \geq \ldots \Gamma_{3(N-1)}$. The two sets of disks are then separated by defining the following Gerschgorin Disk Estimator function :

$$GDE(q) = c_q - \frac{D(Q)}{3(N-1)} \sum_{i=1}^{3(N-1)} c_i, \tag{26}$$

where q=1, …, 3(N-1). $D(Q)$ is an adjustable parameter whose value tends to 0 as the number of snapshots $Q \to \infty$. $D(Q)$ may be selected as $D(Q) = \frac{\kappa}{\ln Q}$, where κ is a positive number whose value is generally less than ln$Q$, and ln(.) denotes natural logarithm. The number of sources is estimated as

$$\hat{J} = q_0 - 1, \tag{27}$$

where q_0 is the smallest integer value of p for which the function GDE(q) is negative. This estimate is based on the assumption that the source number J is such that $J \leq 3(N-1)$.

In summary, the Gerschgorin disk estimator algorithm for an AVS array in a shallow ocean can be stated as follows:

1) Calculate $\hat{\mathbf{R}}_{3N}$ using (17)
2) Partition $\hat{\mathbf{R}}_{3N}$ as in (21) to obtain $\hat{\mathbf{R}}_{3(N-1)}$.
3) Perform eigen-decomposition of $\hat{\mathbf{R}}_{3(N-1)}$ to obtain the eigen-vector matrix $\mathbf{U}_{3(N-1)}$.
4) Construct the matrix $\mathbf{T}$ using (22).
5) Calculate the transformed matrix $\mathbf{R}_T$ using (23).
6) Calculate the radii of Gerschgorin disks using (25).
7) Estimate the number of sources from (27).

In the case of an APS array, $3N$ and $3(N-1)$ are replaced respectively by N and $N-1$ in the foregoing description, the $3(N-1)\times 3$ matrix Γ degenerates to a $(N-1)\times 1$ vector, and the 3×3 matrix $\mathbf{B}$ degenerates to a scalar. Also, the condition $J \leq 3(N-1)$ is replaced by $J \leq (N-1)$.

IV. Results and Discussions

We have considered the ocean model described in Section II, with the following parameters. Ocean depth h = 100 m, sound speed in water c = 1500 m/s, sound speed in sediment c_b = 1700 m/s, attenuation in the sediment is 0.2 dB/wavelength, density ratio $\frac{\rho_b}{\rho}$ = 1.5, signal frequency f = 78 Hz, number of sensors N = 6 unless otherwise stated, inter-sensor spacing d= 9.61 m (half-wavelength), HLA depth = 40 m, depth of topmost sensor of VLA = 5 m, range $r^{(j)}$ = 5 km and source depth $z^{(j)}$ = 10 m for all the sources, number of snapshots Q = 300 unless otherwise stated. All the results have been generated from 200 Monte Carlo simulations. We have evaluated the performance of GDE for both AVS and APS arrays. We have also compared the performance of GDE with that of the AIC and MDL estimators for the AVS array. The primary measure of performance is the probability of correct estimation P_c = P($\hat{J}$ = J).

We shall first address the problem of choosing the value of the adjustable parameter $D(Q)$=$\frac{\kappa}{\ln}Q$ in (26). Consider two sources at bearing 40° and 60°. Figure 1 shows plots of P_c versus Q for different values of κ. The SNR for each source is -5 dB in panel 1a and 0 dB in panel 1b. For Q >300, equally good results are obtained over a wide range of values of κ. For smaller Q, the optimal value of κ is κ_{opt} 6.5 for -5 dB SNR and κ_{opt} 5 for 0 dB SNR. Hence κ = 6$\pm$0.5 appears to be a good choice over a wide range of values of SNR and Q.

We shall now compare the performance of GDE-V (for AVS HLA) and GDE-P (for APS HLA). Figure 2 shows the variation of P_c with SNR when 2 sources are present at 5° and 40°. White noise with Gaussian and Laplacian (GG with α=1) distribution are considered. It is seen that the probability of correct estimation declines rapidly from almost 1 to almost 0 when the SNR dips below a certain threshold. This SNR threshold for GDE-V is approximately 5 dB lower than that for GDE-P. This difference is due to the fact the AVS array provides 3 times as many data samples as the APS array. Hence the AVS array performance is approximately 10 $\log_{10}3$ = 4.7 dB higher than that of the APS array. It is also observed that the performance of GDE is not affected by the change in noise distribution.

Figure 3 shows plots of P_c versus number of snapshots Q for white Gaussian noise at 0 dB and -5 dB SNR. All the other conditions are the same as in Fig. 2. It is seen that the performance of GDE-V begins to degrade only when the number of snapshots is less than 100 even at the low SNR of -5 dB. The performance of GDE-P is significantly poorer in comparison.

Next we compare the performance of GDE-V and GDE-P for HLA in white Gaussian noise when three sources are present at 5°, 30°, and -30° bearing. The source at 30° is termedas the source in the port direction while that at -30° is termed as the source in the starboard direction. Table **I** shows the probability distribution of the estimate $\hat{J}$, i.e. P($\hat{J}$=j), for GDE-P and GDE-V for SNR= -10 dB, 0 dB and 10 dB. It is observed that GDE-P fails to estimate the number of

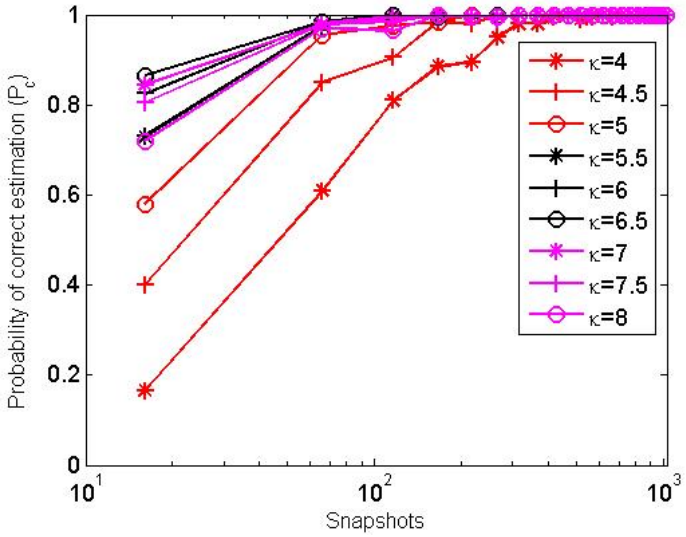

(a) SNR = -5 dB

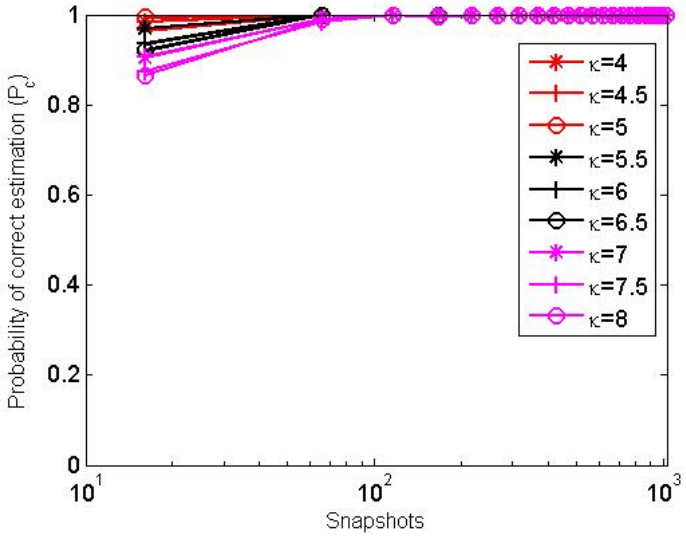

(b) SNR = 0 dB

Figure 1: Probability of correct estimation P_c vs. number of snapshots for GDE-V, considering different values for κ; two sources are located at 40°, 60°.

sources correctly even at high values of SNR. When the SNR is sufficiently high, GDE-P declares only two acoustic sources since the port and starboard sources at 30° and -30° are treated as a single source. GDE-V is able to resolve the port-starboard ambiguity due to its ability to measure acoustic pressure as well as the particle velocity vector; and hence it estimates the number of sources correctly with probability 1 when SNR exceeds -5 dB.

In the next experiment we consider four sources at 10°, 50°, 70° and 110°, all other conditions remaining the same. For this case, the probability distribution of $\hat{J}$ for GDE-P and GDE-V are tabulated in Table **II** for three different values of SNR. In this case, the inability of GDE-P to estimate the number of

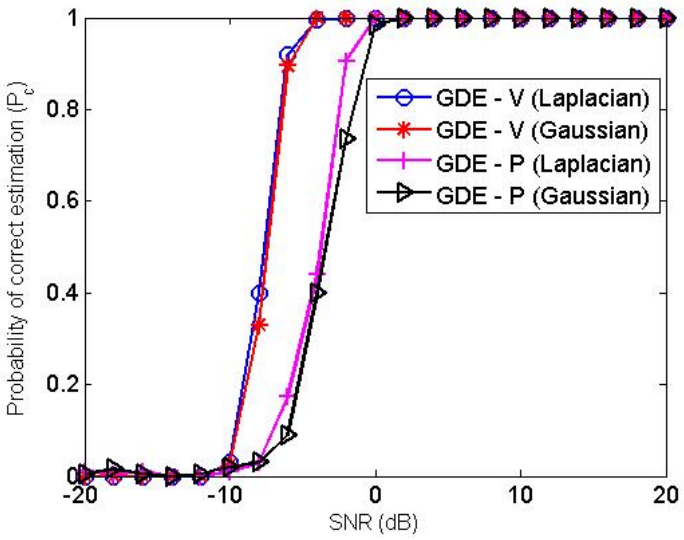

Figure 2: Probability of correct estimation P_c vs. SNR for two sources at 5° and 40°.

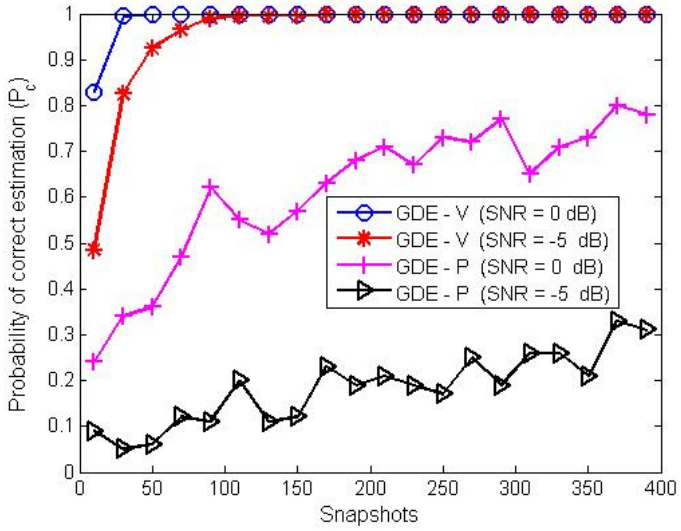

Figure 3: Probability of correct estimation P_c vs. number of snapshots for two sources at 5° and 40°.

j	GDE-P -10 dB SNR	GDE-P 0 dB SNR	GDE-P 10 dB SNR	GDE-V -10 dB SNR	GDE-V 0 dB SNR	GDE-V 10 dB SNR
0	0.17	0	0	0	0	0
1	0.055	0	0	0	0	0
2	0.345	1	1	0.025	0	0
3	0.430	0	0	0.885	1	1
4	0	0	0	0.09	0	0
5	0	0	0	0	0	0

TABLE I: Performance comparison of GDE-P and GDE-V to illustrate resolution of port-starboard ambiguity by GDE-V. Probability distribution P($\hat{J}$ = j) is shown for different SNR.

sources correctly even at high SNR stems from the fact that the number of sensors is too small. As stated in Section III, $J \leq N-1$ and $J \leq 3(N-1)$ are the necessary conditions for the validity of GDE-P and GDE-V respectively. In the present example, GDE-P performs poorly because J is very close to the upper limit of N-1 for the APS array. GDE-V performs very well at -5 db SNR and fairly well even at -10 db SNR since J is well below the upper limit of $3(N-1)$ for the AVS array.

j	GDE-P -10 dB SNR	GDE-P 0 dB SNR	GDE-P 10 dB SNR	GDE-V -10 dB SNR	GDE-V 0 dB SNR	GDE-V 10 dB SNR
0	0.82	0.61	0.565	0	0	0
1	0	0	0	0	0	0
2	0	0.02	0.035	0	0	0
3	0.18	0.37	0.4	0.115	0.04	0.005
4	0	0	0	0.880	0.96	0.995
5	0	0	0	0.005	0	0

TABLE II: Performance comparison of GDE-P and GDE-V to illustrate the ability of GDE-V to estimate a larger number of sources. Probability distribution P($\hat{J}$ = j) is shown for different SNR.

We shall now investigate the effect of varying the number of sensors N on the performance of GDE-V. Consider an AVS HLA in white Gaussian noise and two sources at 5° and 30°. Figure 4 shows plots of P_c versus SNR for Q = 100 snapshots and 3 different values of N. Figure 5 shows plots of P_c versus Q for -5 dB SNR and 3 different values of N. Figure 6 shows the variation of P_c with N for Q = 50 and -5 dB SNR. These figures illustrate the improvement in performance due to increase in the number of sensors.

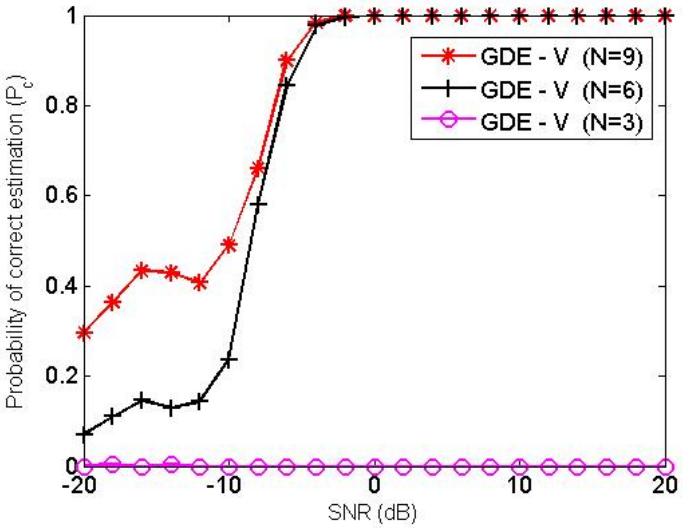

Figure 4: Probability of correct estimation P_c vs. SNR for GDE-V for two sources at 5° and 30°, for 3 different values of N; $Q = 100$

Next, we shall conduct two experiments to compare the capability of different estimators to resolve closely spaced

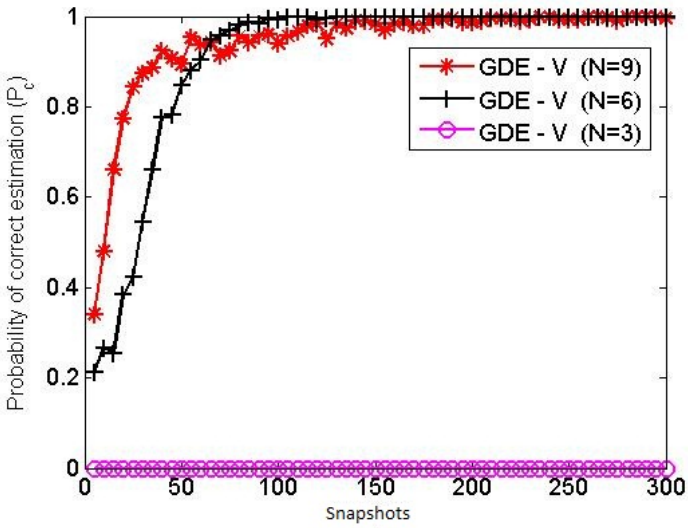

Figure 5: Probability of correct estimation P_c vs. number of snapshots for GDE-V for two sources at 5° and 30°, for 3 different values of N; SNR of each source = -5 dB.

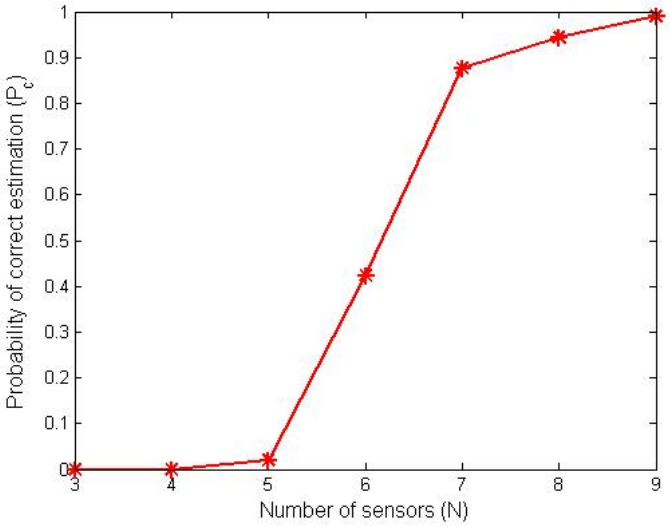

Figure 6: Probability of correct estimation P_c vs. number of sensors (N) for GDE-V for two sources at 5° and 30°; SNR of each source = -5 dB, 50 snapshots.

sources. In the first experiment, we consider two sources at the same range (5 km) and depth (10 m), one source is fixed at a bearing of 50°, and the bearing of the other source is varied from 40° to 60° in steps of 1°. In the second experiment, two sources are at the same bearing (30°) and depth (10 m), one source is fixed at a range of 4 km and the other source is moved away from the first in steps of 200 m. In both experiments, noise is white Gaussian and SNR is 5 dB for both sources. Figure 7 shows plots of P_c versus angular separation, and Fig. 8 shows plots of P_c versus range separation, for GDE-V, GDE-P, AIC and MDL estimators. Since AIC and MDL are implemented only for the AVS array, we do not use the suffix V for these estimators. It is seen from Fig. 8 that GDE-V provides superior bearing resolution compared to the other estimators. GDE-V can resolve two sources if their angular separation is 5° or more. On the other hand, Fig. 8 indicates that none of the estimators can resolve sources at the same bearing even if they are well separated in range.

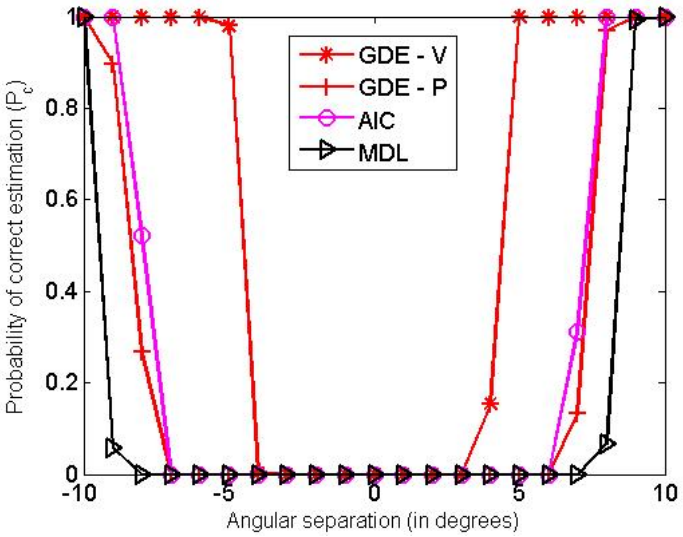

Figure 7: Probability of correct estimation P_c vs. angular separation. Two sources; one at 50° and other varied from 40° to 60°; SNR of each source = 5 dB.

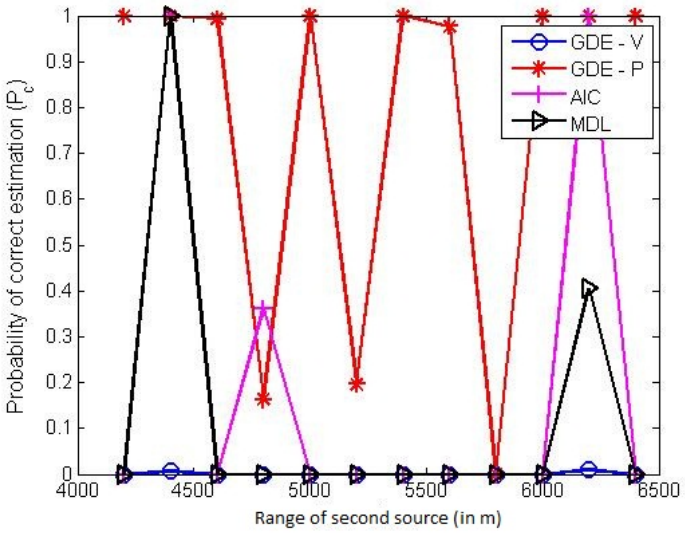

Figure 8: Probability of correct estimation P_c vs. range separation for two sources at the same bearing (30°). One source is at 4000 m and the second is at a larger range.

We shall now compare the performance of GDE-V with the AIC and MDL estimators in greater detail. Consider two sources at 5° and 30°, and white Gaussian noise. Figure 9 shows plots of P_c versus SNR for Q = 300 snapshots, and Fig. 10 shows plots of P_c versus Q for SNR = -4 dB. Figure

11 shows plots of P_c versus Q for SNR = -3 dB if three sources are present at 5°, 30° and 60°. These figures demonstrate that GDE-V outperforms AIC and MDL if SNR is low and/or the number of snapshots is small.

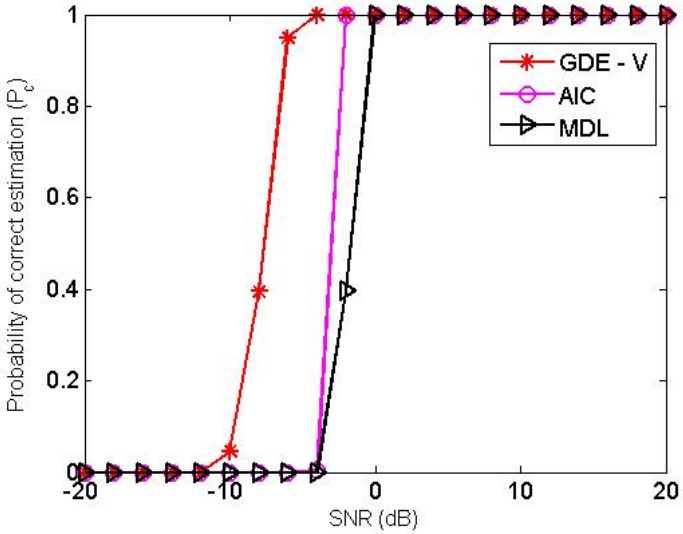

Figure 9: Probability of correct estimation P_c vs. SNR, for GDE-V, AIC and MDL. Two sources are located at 5° and 30°.

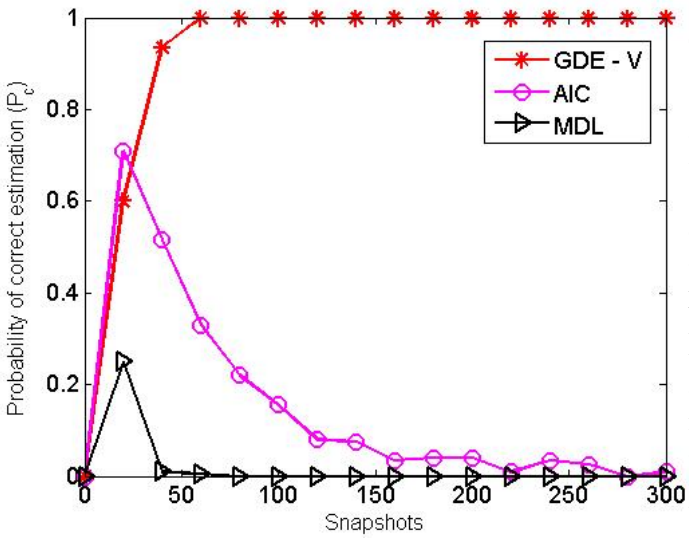

Figure 10: Probability of correct estimation P_c vs. number of snapshots Q, for GDE-V, AIC and MDL. Two sources are located at 5° and 30°; SNR of each source = -4 dB

We shall next compare the performance of the estimators in coloured noise. We model the noise as a Gaussian AR (1) process whose model equation is given by

$$w(t) = a_1 w(t-1) + u(t),\ |a_1| < 1, \tag{28}$$

where $u(t)$ is a Gaussian white noise process and a_1 is a measure of correlation between adjacent samples. Figures 12a and 12b show plots of P_c versus a_1 for two different values of SNR. It is seen that AIC and MDL estimators suffer a drastic degradation in performance as noise correlation increases. GDE-V is significantly more robust compared to the other methods.

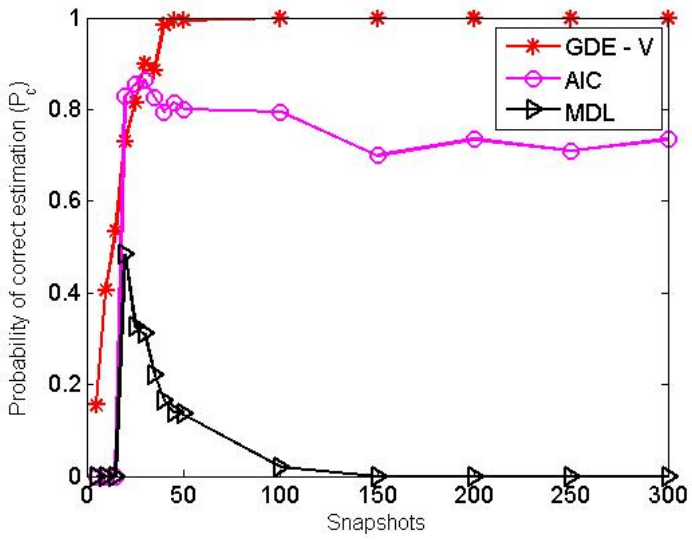

Figure 11: Probability of correct estimation P_c vs. number of snapshots for GDE-V, AIC and MDL; three sources are located at 5°, 30°,60°; SNR of each source = -3 dB

All the foregoing discussion pertains to source number enumeration using an HLA. We shall now consider the use of an AVS VLA. A VLA differs from an HLA in two respects. One obvious difference is the difference in orientation. The other difference is that noise is spatially correlated for a VLA whereas it is spatially uncorrelated for an HLA. Figure 13 shows plots of P_c versus number of snapshots Q for two different values of SNR viz. 5 dB and -5 dB. A comparison of GDE-V (-5 dB) plot in Fig. 13 with the GDE-V (N = 6) plot in Fig. 5 indicates that the performance of GDE-V with AVS VLA is not as good as with AVS HLA. But it is seen that GDE-V provides satisfactory performance if the number of snapshots is sufficiently high. AIC and MDL estimators fail totally even at higher SNR due to the spatial correlation of noise.

V. Conclusion

In this paper, the performance of Gerschgorin disk estimator (GDE) method of source number estimation was investigated in a shallow range-independent ocean. A data model based on the normal mode theory of underwater acoustic propagation was used. Uniform horizontal linear arrays of acoustic pressure sensors (APS) as well as acoustic vector sensors (AVS) were considered. It was shown that the performance of AVS arrays is better than that of the APS arrays in several ways. AVS arrays offer the advantages of a lower noise threshold, higher resolution, elimination of port-starboard ambiguity, and ability to estimate a larger number of sources for a given array size.

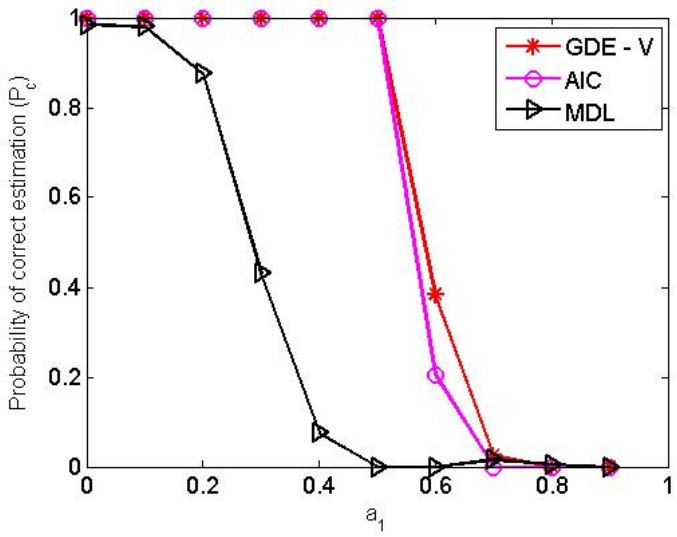

(a) SNR = -1 dB

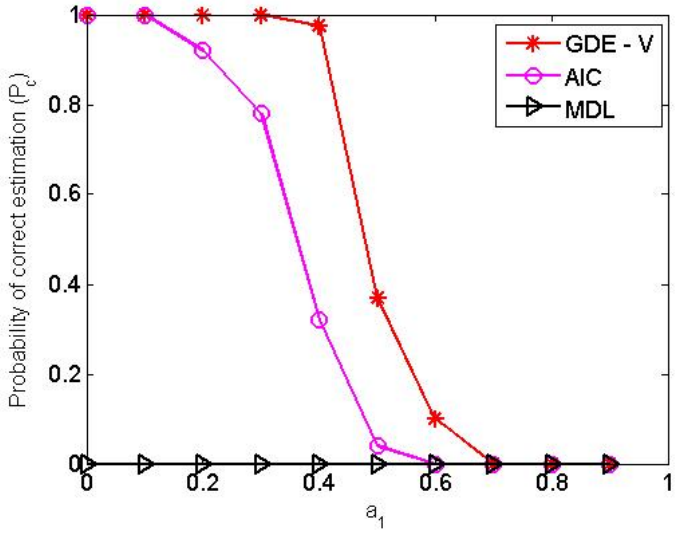

(b) SNR = -3 dB

Figure 12: Probability of correct estimation P_c vs. parameter a_1 of AR (1) noise for GDE-V, AIC and MDL; two sources are located at 5° and 30°.

Conversely, the size of an AVS array required to achieve a prescribed level of performance is only $\frac{1}{3}$ the size of an APS array, and this is a major advantage in several applications such as autonomous underwater vehicles.

GDE is more robust than conventional methods such as AIC and MDL estimators in several ways. GDE provides a significantly better performance at low SNR and/or smaller sample size. Unlike the latter methods, the applicability of GDE is not restricted to white Gaussian noise. GDE can be used for source enumeration in correlated noise since the performance of GDE degrades very slowly with increase in noise correlation. For the same reason, GDE can be used with a vertical AVS array which is situated in a spatially correlated

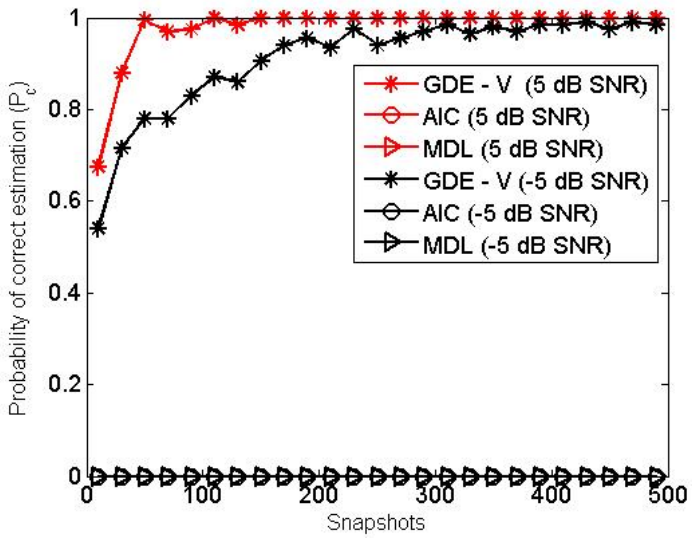

Figure 13: Probability of correct estimation P_c vs. number snapshots for GDE-V, AIC and MDL with an AVS VLA; two sources are located at 5°, 30°.

noise field. GDE also offers a higher bearing resolution than the other estimators. However all the estimators have one common limitation; none of them resolve sources at the same bearing even if they are well separated in range. This issue needs further investigation.

Acknowledgments

This work was partially supported by a grant from National Institute of Ocean Technology, Chennai, India, under the Ocean Acoustics Programme.

Appendix

Probability Density Function of a Complex circular Generalized Gaussian Random Variable

Consider a complex circular GG random variable $X = \bar{X} + j\tilde{X}$, with mean $E[X] = 0$ and variance $var(X) = E[|X|^2] = \sigma^2$.The PDF of X is given by

$$\begin{aligned} f_X(x) = f_{\bar{X},\tilde{X}}(\bar{x},\tilde{x}) &= B(\alpha)e^{-C(\alpha)|x|^\alpha} \\ &= B(\alpha)e^{-C(\alpha)(\bar{x}^2+\tilde{x}^2)^{\alpha/2}} > 0 \end{aligned} \tag{29}$$

The constants $B(\alpha)$ and $C(\alpha)$ can be determined by invoking the constraints

$$\int_{-\infty}^{\infty}\int_{-\infty}^{\infty} f_{\bar{X},\tilde{X}}(\bar{x},\tilde{x})d\bar{x}d\tilde{x} = 1 \tag{30}$$

$$\begin{aligned} E[|X|^2] &= \int_{-\infty}^{\infty}\int_{-\infty}^{\infty}(\bar{x}^2+\tilde{x}^2)f_{\bar{X},\tilde{X}}(\bar{x},\tilde{x})d\bar{x}d\tilde{x} \\ &= \sigma^2 \end{aligned} \tag{31}$$

On substituting (29) into (30) and performing the integration, we get

$$\frac{8\pi BC^{-2/\alpha}}{\alpha}\Gamma(\frac{2}{\alpha}) = 1, \tag{32}$$

where $\Gamma(.)$ denotes the gamma function. On substituting (29) into (31) and performing the integration, we get

$$\frac{8\pi BC^{-4/\alpha}}{\alpha}\Gamma(\frac{4}{\alpha}) = \sigma^2. \tag{33}$$

From (32) and (33), we get

$$B = \frac{\alpha\Gamma(\frac{4}{\alpha})}{8\pi\sigma^2[\Gamma(\frac{2}{\alpha})]^2}, \tag{34a}$$

$$C = \frac{1}{\sigma^\alpha}\left(\frac{\Gamma(\frac{4}{\alpha})}{\Gamma(\frac{2}{\alpha})}\right)^{\alpha/2}. \tag{34b}$$

It can be easily shown that X satisfies the following properties of circular random variables:

$$E[\bar{X}^2] = E[\tilde{X}^2] = \frac{1}{2}E[\bar{X}^2 + \tilde{X}^2] = \frac{1}{2}\sigma^2, \tag{35}$$

$$E[\bar{X}\tilde{X}] = 0 \tag{36}$$

It may be noted that the marginal PDFs of $\bar{X}$ and $\tilde{X}$ *are not* generalized Gaussian.

References

[1] R. O. Schmidt, "Multiple emitter location and signal parameter estimation." In *Proceedings of RADC Spectrum Estimation Workshop,* Rome Air Development Center, Rome, pp. 243-258, 1979.

[2] R. Roy and T. Kailath, "ESPRIT- Estimation of Signal Parameters via rotational invariance techniques", *IEEE Trans.Acoust., Speech, Signal Process.,* 37(7), pp. 984-995 1989.

[3] M. Wax and T. Kailath, "Detection of signals by information theoretic criteria," *IEEE Trans.Acoust. Speech, Signal Process.,* 33(2), pp. 387-392, 1985.

[4] M. Wax and I. Ziskind, "Detection of the number of coherent signals by the MDL principle," *IEEE Trans. Acoust., Speech, Signal Process.,* 37(8), pp. 1190-1196, 1989.

[5] F. W. Machell, C. S. Penrod and G. E. Ellis, "Statistical characteristics of ocean acoustic noise process", in *Topics in Non-Gaussian Signal Processing*, E. J. Wegman, S. C. Schwartz and J. B. Thomas (Eds.), Springer-Verlag, Berlin, Germany, pp. 29-57, 1989.

[6] D. C. Bertilone and D. S. Killeen, "Statistics of biological noise and performance of generalized energy detectors for passive detection," *IEEE J. Oceanic Engineering*, 26(2), pp. 285-294, 2001.

[7] M. J. Buckingham, "A theoretical model of ambient noise in a low-loss shallow water channel," *J. Acoust. Soc. America,* 67(4), pp. 1186-1192, 1980.

[8] H. T. Wu, J. F. Yang and F. K. Chen, "Source number estimators using transformed Gerschgorin radii," *IEEE Trans. Signal Process.,* 43(6), pp. 1325-1333, 1995.

[9] L. Huang, T. Long and S. Wu, "Source enumeration for high-resolution array processing using improved Gerschgorin radii without eigendecomposition," *IEEE Trans. Signal Process.,* 56(12), pp. 5916-5925, 2008.

[10] Y. Z. Mei and P. Wang, "Estimation of source number using Gerschgorin disks based on acoustic vector sensor array." In *Proceedings of 2010 International Conference on Computer Application and System modelling,* pp. V7-291-V7-295, 2010.

[11] A. Nehorai and E. Paldi, "Acoustic vector-sensor array processing," *IEEE Transactions on Signal Processing,* 42(9), pp.2481-2491, 1994.

[12] M. Hawkes and A. Nehorai, "Wideband source localization using distributed acoustic vector-sensor array," *IEEE Trans. Signal Process.,* 51(6), pp. 1479-1491, 2003.

[13] K. G. Nagananda and G. V. Anand, "Subspace intersection method of high-resolution bearing estimation in shallow ocean using acoustic vector sensors," *Elsevier Signal Processing*, 90(1), pp. 105-118, 2010.

[14] S. Lakshmipathi and G. V. Anand, "Subspace intersection method of high-resolution bearing estimation in shallow ocean," *Elsevier Signal Processing,* 84(8), pp. 1367-1384, 2004.

[15] L. M. Brekhovskikh, Y. P. Lysanov, "Chapter 5" in *Fundamentals of Ocean Acoustics*, 3rd ed., Springer, Berlin, 1991.

[16] N. Suresh Kumar, G. V. Anand, S. Roul and D. J. Philip, "Source number estimation in shallow ocean by acoustic vector sensor array using Gerschgorin disks," In *Proceedings of 12th International Conference on System Design and Applications (ISDA),* 2012.

Author Biographies

N. Suresh Kumar is currently Scientist 'F', Naval Physical and Oceanographic Laboratory, Kochi, Kerala, India. He received his M.E degree in electrical communications from the Indian Institute of Science (IISc), Bangalore, India in 1995. His research areas include under water acoustics, sonar signal processing, compressive sensing and sensor networks.

Dibu John Philip is currently pursuing his M.Tech. degree in Signal Processing at the Mahatma Gandhi University (MGU), Kerala, India. He received the bachelor's degree in electronics and communication engineering from MGU in 2011. His research interests include under water acoustics, machine learning and computer networks.

G. V. Anand received the Ph.D. degree in Engineering from Indian Institute of Science (IISc), Bangalore, in 1971. He served on the faculty of the Department of Electrical Communication Engineering, IISc, from 1969 to 2006. He was a Visiting Academic Staff Fellow at University College, London in 1978-79, Visiting Scientist at Naval Physical and Oceanographic Laboratory, Kochi, India in 1996-97, and Visiting Professor in University of Angers, France in 2002, and Cankaya University, Ankara, Turkey in 2003-04. He is currently Visiting Professor at IISc and the MRD Chair Professor at PES Institute of Technology, Bangalore. He is a Fellow of Indian Academy of Sciences, Indian National Academy of Engineering, Institution of Electronics and Communication Engineers, India, and Acoustical Society of India. His research interests include statistical signal processing, ocean acoustics and nonlinear dynamics.